Investigating the stability of fine-grain digit somatotopy in individual human participants

Abbreviated title: Stable fine-grain somatotopy in human SI.

James Kolasinski[1,2*], Tamar R. Makin[1], Saad Jbabdi[1], Stuart Clare[1], Charlotte J. Stagg[1,3], Heidi Johansen-Berg[1]

1. Oxford Centre for fMRI of the Brain, Nuffield Dept. of Clinical Neurosciences, University of Oxford, UK, OX3 9DU
2. University College, Oxford, UK OX1 4BH
3. Oxford Centre for Human Brain Activity, Department of Psychiatry, University of Oxford, Oxford, UK, OX3 7JX
* Corresponding author

Number of pages: 35
Number of figures: 8

Word counts
Abstract: 235
Introduction: 619
Materials and Methods: 2463
Results: 1522
Discussion: 1498
References: 2347 (88 entries)
Figure legends: 1132

Conflict of interest: The authors declare no competing financial interests.

Acknowledgements
JK holds a Stevenson Junior Research Fellowship at University College, Oxford. TM and CJS both hold Wellcome Trust/Royal Society Henry Dale Fellowships. SJ holds an MRC Career Development Fellowship (TRM Grant Number 104128/Z/14/Z). HJB holds a Wellcome Trust Senior Research Fellowship. The work was additionally supported by the NIHR Oxford Biomedical Research Centre. Support for the 7T scanner was provided by the Medical Research Council. The authors thank Adam Thomas for his assistance with fMRI analysis.

ABSTRACT

Studies of human somatosensory cortex have placed a strong emphasis on the cortical representation of the hand and the propensity for plasticity therein. Despite many reports of group differences and experience-dependent changes in cortical digit somatotopy, relatively little work has considered the variability of these maps across individuals, and to what extent this detailed functional architecture is dynamic over time. With the advent of 7-tesla fMRI, it is increasingly feasible to map such detailed organisation non-invasively in individual human participants. Here we extend the ability of ultra-high field imaging beyond a technological proof of principle to investigate the inter-subject variability of digit somatotopy across participants, and the stability of this organisation across a range of intervals. Using a well-validated phase-encoding paradigm and an active task, we demonstrate the presence of highly reproducible maps of individual digits in SI, sharply contrasted by a striking degree of inter-subject variability in the shape, extent and relative position of individual digit representations. Our results demonstrate the presence of very stable fine-grain somatotopy of the digits in human SI, and raise the issue of population variability in such detailed functional architecture of the human brain. These findings have implications for the study of detailed sensorimotor plasticity in the context of both learning and pathological dysfunction. The simple task and 10-minute scan required to derive these maps also raises the potential for this paradigm as a tool in the clinical setting.

SIGNIFICANCE STATEMENT

We apply ultra-high resolution fMRI at 7 tesla to map sensory digit representations in the human cortex at the level of individual participants across multiple time points. The resulting fine-grain maps of individual digits in somatosensory cortex reveal both the stability in this fine-grain functional organization over time, contrasted with the variability in these maps across individuals.

INTRODUCTION

The somatotopic organization of primary somatosensory cortex is well established in the human brain, both at the level of whole-body topography (Penfield and Boldrey, 1937; Walter et al., 1992; Zeharia et al., 2015) and the more fine grain organisation in the representations of the face and the hand (Moulton et al., 2009; Sanchez-Panchuelo et al., 2010). The somatotopic digit map is the subject of continuing interest, with its relative cortical overrepresentation (Mountcastle, 2005). More generally, its is increasingly clear that SI plays a critical role in motor function (Vidoni et al., 2010; Platz et al., 2012; Jacobs et al., 2014).

Studies of human somatotopy have focused considerable effort on attempting to map the representations of digits in the cortex (Baumgartner et al., 1991; Gelnar et al., 1998; Kurth et al., 1998; Francis et al., 2000; Overduin and Servos, 2004; Nelson and Chen, 2008; Schweizer et al., 2008) and the cerebellum (van der Zwaag et al., 2013). Further work has provided evidence for marked topographical differences in the cortical spacing and organisation of SI somatotopy in specific sub-populations, for example in musicians and individuals with focal dystonia (Bara-Jimenez et al., 1998; Elbert et al., 1998; Meunier et al., 2001; Butterworth et al., 2003; Nelson et al., 2009). Other studies, chiefly using MEG, report a propensity for experience-dependent plasticity in SI somatotopy (Braun et al., 2000; Schwenkreis et al., 2001; Candia et al., 2003; Stavrinou et al., 2007; Vidyasagar et al., 2014), building upon seminal studies undertaken in non-human primates (Allard et al., 1991; Zarzecki et al., 1993). However the spatial

resolution of both MRI and MEG is typically insufficient to make a strong argument about fine-grain digit somatotopy in the somatosensory hand area.

With the increasing prevalence of 7-tesla MRI scanners, it is now possible to resolve SI representations of all of the digits in the hand at the level of individual participants. A number of elegant studies at ultra-high field have used tactile stimulation to demonstrate not only the ability to map digit somatotopy in SI with a number of paradigms, but also the existence of within-digit somatotopy and cortical overlap between adjacent digit pairs (Sanchez-Panchuelo et al., 2010; 2012; Besle et al., 2013a; 2013b)

Reports of SI digit maps to date have showcased the novel capabilities of ultra-high field fMRI (Sanchez-Panchuelo et al., 2012; Besle et al., 2013a; 2013b; Martuzzi et al., 2014; Stringer et al., 2014). In light of the considerable interest in cortical digit maps, and specifically their capacity for plasticity, more thorough cross-sectional and longitudinal analyses are necessary.

While non-human primate data demonstrates considerable inter-subject variability in SI digit somatotopy (Merzenich et al., 1987), little evidence exists to demonstrate stability of the shape and position of SI digit maps over time. Human studies to date have only considered the reproducibility of isolated individual digit representations, or used relatively crude measurements (e.g. centre of mass) (Vidyasagar and Parkes, 2011; Martuzzi et al., 2014). It therefore remains unclear to what extent reports of inter-subject variance in primates could actually reflect intra-individual instability in digit representations in SI. In

order to meaningfully interpret previous reports of use-dependent plasticity and group variability in human cortical digit representations, it is vital to develop a more thorough understanding of SI digit somatotopy in the healthy population.

Here we address this fundamental gap in the literature, using 7T fMRI mapping to explore the fine grain functional organization of SI at the level of individual human participants. More specifically, we apply a phase-encoding paradigm well-validated for sensory body mapping (Sereno and Huang, 2006; Orlov et al., 2010; Sanchez-Panchuelo et al., 2010; Mancini et al., 2012; Zeharia et al., 2015) to investigate whether stable and reproducible maps of individual digits exist in human SI.

Materials and Methods

Participants

Thirteen healthy control participants [Table 1; Mean age: 28.6 ± 5.66; six female] were recruited in accordance with local central university research ethics committee approval (University of Oxford; MSD-IDREC-C2-2013-05). All participants were right handed according to the Edinburgh Handedness Inventory (Oldfield, 1971).

Experimental design

Participants attended three scan sessions. Two of the sessions were separated by a period of 24 hours (0 hours and +24 hours). The third session took place four weeks before or after the other two sessions. During each session participants

underwent a one-hour fMRI scan. One of the sessions also involved an additional scan to acquire a structural image.

MRI acquisition

Functional MRI data were acquired using a Siemens 7T Magnetom system with a 32-channel head coil. An initial functional localiser scan was used to identify hand movement-related activity in order to aid slice placement for subsequent task fMRI scans (Multislice gradient echo EPI, TR: 3000ms, TE: 25ms, flip angle: 90, bandwidth: 1568Hz, 43 axial slices, 2x2x2mm resolution, GRAPPA factor = 2). Task fMRI data were then acquired using a field of view based on the results of the functional localizer; true axial slices were centred on the hand knob activation in the z-axis of the left hemisphere (Multislice gradient echo EPI, TR: 1500ms, TE: 25ms, flip angle: 90°, bandwidth: 1562Hz, 22 axial slices, 1.2x1.2x1.2mm resolution, GRAPPA factor = 2).

For image registration purposes, single volume high-saturation EPI images were acquired: one whole brain image and one partial field of view (FOV) image with the same slice placement as the task fMRI. T1-weighted Multi-Echo Magnetization Prepared Rapid Acquisition Gradient Echo (MEMPRAGE) structural scans were acquired during one of the three sessions (van der Kouwe et al., 2008) using a 3T Siemens Trio system (TR: 2530ms, TE: 1.69, 3.55, 5.41 and 7.27ms, 1x1x1 mm, GRAPPA factor = 2).

fMRI tasks

Participants performed a series of tasks involving visually-cued movements of individual digits in the scanner: digit 2 (D2: index finger), digit 3 (D3: middle finger), digit 4 (D4: ring finger) and digit 5 (D5: little finger). An active motor task was selected to optimally activate a range of inputs to the cortical somatosensory system, analogous to daily use of the hand. Movement recruits a combination of peripheral receptors encoding a range of somaesthetic modalities, from surface mechanoreceptors to deeper cutaneous receptors and proprioceptors, as well as efference information from the motor system.

During the three minute functional localiser scan, participants were instructed to appose their right thumb with each of the digits of their right hand sequentially during 15 second movement blocks, contrasted with equivalent periods of rest. All subsequent task fMRI involved individual movements of D2, D3, D4 and D5 in the form of button presses using an MRI-compatible four-finger button-box (manufactured in-house) resting on the participant's right thigh during the scan. Participants were presented with four white circles, corresponding to the four digits of the right hand, shown on a visual display projected into the scanner bore. The displayed circles flashed individually at a constant frequency to cue participants to make button presses at the specified rate. Further discussion of the caveats associated with using an active motor task in the study of somatosensory cortex are outlined in *Limitations* below.

A phase-encoding task was used, which involved continuous button presses with no rest periods (Figure 1A). The task consisted of movement blocks of 8 seconds in duration, during which participants moved one digit (D2-D5) at a rate of 1 Hz.

The phase-encoding forward task cycled through blocks of D2, D3, D4 and D5 in a repeating sequence (8 repetitions of the cycle; Figure 1A). The phase-encoding backwards task cycled through blocks of D5, D4, D3 and D2 in a repeating sequence (8 repetitions of the cycle). The total duration of the phase-encoding task was 8 mins 50 secs. The activation maps derived from the phase-encoding forward and backward tasks were averaged voxel-wise; further details below.

A standard block task was also undertaken, which involved movement blocks and rest blocks, both 12 seconds in duration. A total of four movement blocks were acquired per digit (16 movement blocks total), in a counterbalanced order, randomized across visits. During movement blocks, participants were instructed to perform movements of a specific digit at 1 Hz (e.g. D2, D2, D2, D2 . . .). Each movement block was separated by a rest block. The total duration of the block task was 6 mins 24 secs.

MRI analysis

MRI analysis was undertaken using tools from FSL and Connectome Workbench (Smith et al., 2004; Woolrich et al., 2009; Marcus et al., 2011; Jenkinson et al., 2012). MRI data were projected to cortical surface reconstructions produced with FreeSurfer T1-weighted MEMPRAGE images (Dale et al., 1999; Fischl et al., 2001).

MRI preprocessing

All fMRI data were subject to the following preprocessing steps: motion correction using MCFLIRT (Jenkinson et al., 2002); removal of non-brain tissue

using the Brain Extraction Tool (BET) (Smith, 2002), high pass temporal filtering (Gaussian-weighted least squares straight line fitting with sigma = 100 seconds) and spatial smoothing using a Gaussian kernel of FWHM 1.5 mm.

Image registration

Image registration was undertaken within participant using FLIRT (Jenkinson and Smith, 2001; Jenkinson et al., 2002) and Freesurfer's Freeview. Task fMRI data from the three scan sessions were first registered to a partial-FOV high-saturation EPI image acquired during an additional scan session to avoid biasing any single time point (6 degrees of freedom, normalized correlation cost function). The partial-FOV high-saturation EPI image was then registered to the T1-weighted MEMPRAGE image using boundary-based registration (BBR) (Degrees of freedom: 6, FMRIB's Automated Segmentation Tool (FAST) white matter segmentation, no search) (Greve and Fischl, 2009), initialised with an affine registration matrix. The results of the BBR were used as a starting point for manual alignment of the single volume partial-FOV high-saturation EPI image to the structural MEMPRAGE white matter and pial surfaces using blink comparison as implemented in Freeview, an approach applied previously in studies of fine-grain topography (Mancini et al., 2012).

Phase-encoding analysis

The phase-encoding task fMRI data were analysed using a cross-correlation approach previously applied in retinotopy, and more recently for body mapping (Engel et al., 1997; Wandell et al., 2007; Orlov et al., 2010); see *Limitations* for further discussion. This analysis used cross-correlation to find the time point in

239 the phase-encoding forward (D2-D5) and phase-encoding backwards (D5-D2)
240 tasks at which each cortical voxel responded maximally.
241
242 To achieve this, the preprocessed BOLD EPI data were correlated against a series
243 of reference models. The model was composed of a gamma-convolved boxcar: 8
244 second 'on' and 24 second 'off', repeated eight times, mirroring the eight 32-
245 second cycles of the phase forward and phase backward tasks (Figure 1B: black).
246 The model was shifted in time iteratively by a number of lags so that activity
247 throughout the cycle could be modeled (Figure 1B). This approach increases
248 sensitivity to track a wave of activation (Engel, 2012), in this case associated
249 with the cycles of movement which progress either from D2-D5, or D5-D2. A
250 correlation was calculated between the raw BOLD signal of each voxel (Figure
251 1B: red) and the reference model at each lag (Figure 1B: black). Each iteration
252 shifted the model by a given lag (1.5 seconds). With each lag the 8 second 'on' of
253 each 32 second cycle was time shifted (e.g. model 1: 8s on/24s off; model 2: 1.5s
254 off/8s on/22.5s off; model 3: 3s off/8s on/21s off …), with sufficient shifts to
255 cover one 32-second cycle. By plotting for each voxel the cross-correlation at
256 each voxel as a function of the lag, a tuning curve was created for each voxel,
257 demonstrating the optimal model fit for that voxel (Figure 1C). Each lag was
258 assigned to a given digit in the cycle. Voxels responsive to a particular digit
259 demonstrate a peak cross-correlation within the lags corresponding to
260 movement that digit in the cycle.
261
262 For each participant and session, the *r*-values resulting from the cross-
263 correlation analysis specified above (Figure 1C) were averaged across the lags

assigned to the same digit to yield digit maps (D2, D3, D4, D5) for each of the phase-encoding forward and phase-encoding backwards tasks. For each participant and each session, the maps for each digit from the phase-encoding forward and phase-encoding backward tasks were resampled to the single volume partial FOV high-saturation EPI space and averaged to give a single voxel-wise *r*-value map for each session and for each digit (Figure 1D). For each participant, session and digit, a corresponding voxel-wise *z*-statistic map was calculated on the basis of the distribution of values within the brain tissue of the FOV for which BOLD EPI data were acquired. These soft-edged maps were further masked using a winner-take-all approach to produce digit maps in which each voxel was assigned exclusively to one digit.

Block task analysis

The block task fMRI data were analysed using a GLM in the FMRIB Expert Analysis Tool (FEAT). All analysis was undertaken on the single-participant level, using FMRIB's Improved Linear Model (FILM) to estimate timeseries autocorrelation and pre-whiten each voxel. Each digit was modeled with a separate boxcar regressor with gamma-HRF convolution and its temporal derivative, giving a total of eight regressors. FEAT was used to produce activation maps corresponding to each of the four digits by contrasting a given digit regressor to the rest blocks (e.g. D2 > rest).

Surface projection

Phase-encoding winner-take-all *z*-statistic digit maps were projected to two-dimensional surface space using a cortical ribbon mapping method implemented

289 in Connectome Workbench. This approach estimates the contribution of multiple
290 voxels to one point on the cortical surface and weights the values therein
291 accordingly.
292
293 For visualization on the cortical surface of individual participants, winner-take-
294 all *z*-statistic maps for each digit and time point were thresholded using FDR to
295 determine a corrected *p*-value threshold on the basis of the observed *p*-value
296 distribution within the data (α=0.001) (Genovese et al., 2002). This resulted in
297 individually defined FDR thresholds for each map under consideration (Table 2).
298
299 For inter-subject comparison, volumetric winner-take-all *z*-statistic maps were
300 resampled into atlas space using Combined Volumetric and Surface (CVS)
301 registration to achieve accurate and robust alignment with the CVS atlas
302 (Postelnicu et al., 2009), and projected to the atlas two-dimensional surface
303 using the cortical-ribbon mapping method.
304
305 *Intra-subject reproducibility*
306 The Dice coefficient (Dice, 1945) was used to assess the reproducibility of phase-
307 encoding digit maps over time, quantifying the spatial similarity of digit map
308 areas. The Dice coefficient varies from 0 (no overlap between digit maps) to 1
309 (perfect overlap between digit representations). For each digit, the winner-
310 takes-all digit maps for that digit were thresholded (FDR α=0.001) and overlap
311 was calculated between each possible pairing across each of the three time
312 intervals. Where A and B are the area of the two digit representations, the Dice
313 Coefficient is expressed as:

$$\frac{2 \times |A \cap B|}{|A| + |B|} \quad (1)$$

Inter-subject variability

The variability in the spatial location of individual digit representations across participants was assessed using the Dice coefficient. Surface-area based thresholding was applied to the winner takes digit maps, such that the maximal 80mm^2 of activation within SI for a specific digit was considered. Digit representations with this surface area were present within S1 for every participant and time point. The interpretability of a Dice coefficient (Equation 1) calculated across different subjects could be affected by inter-subject differences in the size of digit representations. The use of a fixed surface area for each digit representation excluded any effect of inter-subject variability in the spatial size of digit maps on inter-subject comparisons. Each winner-takes-all digit representation at time point 0 hour was compared with each other winner-takes-all digit representation at time point +/- 4 weeks across all participants.

Dice coefficients were used to construct a large inter-subject Dice comparison matrix (36 x 36 cells), composed of submatrices (9 x 9 cells) for all possible digit pairings. To compare digit representation overlap intra-subject (submatrix diagonal), to digit representation overlap inter-subject (submatrix off-diagonals), measures of matrix dominance ratio (Mdr) were calculated for each submatrix (Greene and Cunningham, 2006). The Mdr of a square matrix *K,* of width and height *n* can be expressed as:

$$(2) \quad \frac{\frac{1}{n}\sum_i K_{ii}}{\frac{1}{n(n-1)}\sum_{i,j,i\neq j} K_{ij}}$$

Values of Mdr greater than one would therefore be observed in cases where the average Dice overlap of two digit representations within the same subjects (the matrix diagonal) is of greater magnitude than the average Dice overlap made across different subjects (the matrix off-diagonals).

A higher-level matrix of the Mdr values for each digit pairing was constructed, from which an overall Mdr value was calculated. A high value of overall Mdr in this matrix would suggest high matrix dominance in comparisons of 'same' digits (e.g. D2-D2, D3-D3…) and low levels of matrix dominance in comparisons on 'different' digits (e.g. D2-D3, D3-D5 etc.). This is turn would support the hypothesis that intra-subject overlap in 'same' digits is greater than inter-subject overlap in 'same' digits.

Bootstrap resampling was applied to the large inter-subject Dice comparison matrix (36 x 36 cells) in order to quantify the likelihood of observing the reported pattern by chance, and therefore the statistical significance of the overall Mdr value.

Additional measures of reproducibility and variability

As well as the primary Dice measures of intra-subject reproducibility and intra-subject variability, additional features of the phase-encoding digit maps were

assessed. At each time point soft-edged phase-encoding maps (FDR α=0.01) were used to assess the amount of overlap between different digit representations within S1. These measures sought to characterize the extent of shared cortical territory between different digit representations, which the winner-takes-all maps do not capture, and to assess the consistency in the extent of this overlap at each time point. The extent of this overlapping shared territory was expressed as a Dice coefficient. The pattern of overlap in these soft-edged digit representations was represented in 4x4 matrices for each participant and each time point. The pattern in these matrices were compared using a ranked Mantel test (Mantel, 1967), in order to quantify both the intra-subject consistency in the overlap pattern, and the inter-subject variability therein.

In a complementary analysis, peak z-stat coordinates for each digit were calculated with SI on the inflated cortical surface, allowing for the calculation of geodesic distances between adjacent digits for each time point (D2-D3, D3-D4, D4-D5), which were again assessed for consistency.

Identifying additional digit maps

To increase statistical power in order to identify further somatotopic digit maps previously reported in SI (Pons et al., 1985; Huffman and Krubitzer, 2001; Yau et al., 2013), an additional all-session phase-encoding map was produced by co-registering and averaging the forward and backward lags from all three sessions, before processing the resulting maps as outlined above, using a more liberal FDR threshold (α=0.01).

Statistics

All statistical analysis and graphing were undertaken using JMP (Version 11.0, SAS Institute, Cary, NC, USA) and Statistics Package for the Social Sciences (SPSS, Version 19.0, IBM Corporation, Armork, NY, USA).

RESULTS

All BOLD EPI data were assessed for excessive motion both visually and using motion estimate outputs from MCFLIRT: data from three participants exhibited visible spin history motion artifact as a result of sharp motion during one or more scan sessions (greater than 1mm of absolute mean displacement in fewer than five volumes; Table 1); these participants were excluded. Further analysis found no significant or systematic correlation between the task design and motion parameters in the remaining participants. One further participant was excluded on the grounds of an incidental finding. Nine participants were considered in further analysis [Table 1: Participants 1-9; Mean age: 28.5 ± 6.54; four female; -4 weeks: four participants; +4 weeks: five participants].

Phase-encoding digit maps in SI

The thresholded activation maps from the phase-encoding analysis displayed a clear and specific pattern in the left post-central gyrus around the anatomically characteristic hand knob (Figure 2A/D) (Yousry et al., 1997). Maps showed a pattern of progression from the lateral-most representation of digit two, to the medial most representation of digit five (Figure 2C/D), a pattern that was consistent across all participants and time points (Figure 3/4). However, the maps showed striking qualitative differences in shape and orientation across

participants, in keeping with reports of inter-subject variability from the non-human primate literature (Merzenich et al., 1987).

Activation was isolated to the primary somatosensory cortex on the postcentral gyrus, with minimal extraneous activation within the FOV in which BOLD EPI data were acquired (Figure 2C); no mask or ROI has been applied to any digit maps presented herein. The Brodmann areas that constitute the primary somatosensory cortex cannot be defined accurately on the basis of gross anatomy alone. However, the location of the observed digit representations is broadly anatomically consistent with the location of Brodmann area 3b: on the posterior bank of the central sulcus, posterior to area 3a in the nadir and anterior to area 1 at the apex of the post-central gyrus. Some subjects displayed partial additional maps more posteriorly in regions consistent with Brodmann area 2 or 1 (Figure 3/4: participants 3 and 9).

A post-hoc region of interest (ROI) analysis was used to explore the BOLD signal underlying the phase-encoding digit maps. The average BOLD signal time course was extracted within each digit representation (Z >3.5) (Figure 2B). These showed clear and specific activation patterns in a sequence consistent with the phase-encoding task digit order.

Intra-subject digit map reproducibility over 24 hours and four weeks

Surface-projections of digit maps derived from phase-encoding analysis qualitatively display a striking degree of reproducibility of these fine-grain maps at the single-participant level across both the 24 hour and four week map-remap

intervals (Figure 3/4). To quantitatively assess the intra-individual reproducibility of the phase-encoding derived digit maps, Dice similarity coefficients were used to compare the spatial extent of digit representations across sessions.

A Dice coefficient was calculated between every possible digit pairing and every possible time point pairing (Figure 5A) within a FreeSurfer anatomically defined ROI of SI overlapping the fMRI acquisition volume. This analysis demonstrated a very high degree of spatial concordance between 'same' digit representations across all time intervals.

The reproducibility matrices were averaged across the two different time intervals and further averaged into three digit pairing categories: homologous digits, first order neighbours and second/third order neighbours (Figure 5A; part iv) in order to assess whether the Dice coefficient for homologous digits was significantly greater than the equivalent value between non-homologous digit pairings. A one-way repeated measures ANOVA was performed with one factor of digit pairing category. There was a significant main effect of digit pairing category on the Dice coefficient: $F(2, 19) = 119.429$, $p < .0005$. Post hoc analysis with a Bonferroni adjustment revealed that the Dice coefficient was significantly greater for homologous digit pairings (Average Dice coefficient: 0.542, 95% CI: 0.380 to 0.584) compared with pairings of first order neighbours (Average Dice coefficient: 0.010, 95% CI: 0.000 to 0.020), and pairings of second and third order neighbours (Average Dice coefficient: 0.001, 95% CI: 0.000 to 0.002); all $p < .0005$ (Bonferonni-adjusted). The same pattern of results was also seen using

462 an equivalent analysis approach on volumetric data rather than surface
463 projected data.
464
465 *Inter-subject digit map variability*
466 Consistent with qualitative observations (Figure 3/4), Dice analysis comparing
467 the spatial location of individual digit representations (Figure 5B; part i)
468 demonstrates a considerable degree of inter-subject variability when compared
469 to the consistency seen intra-subject. In comparison of 'same' digits over time
470 (e.g. D2-D2, D3-D3) the degree of overlap observed intra-subject exceeds that
471 observed inter-subject, resulting in values of Mdr >1. This is consistent with the
472 notion of variability in the spatial position of individual digit representations. In
473 contrast, for 'different' comparisons (e.g. D2-D4), the degree of overlap observed
474 inter-subject exceeds the degree of overlap observed intra-subject, yielding
475 values of Mdr <1. This further strengthens our claim that intra-subject
476 consistency is driven by reproducibility of the spatial patterns for the same digits
477 over time, rather than other irrelevant aspects of the map (e.g. geometrical
478 cluster characteristics).
479
480 Values of Mdr for each digit comparison are summarized in Figure 5B(ii). From
481 this matrix a value of overall Mdr was calculated at 19.67 (Equation 2; Average
482 Mdr for 'same' digit pairings / Average Mdr for 'different' digit pairings). In order
483 to substantiate the observed pattern and value of overall Mdr yielded, we applied
484 bootstrap resampling to the inter-subject Dice comparison matrix (50,000
485 iterations) to account for the likelihood of observing this value by chance (Figure
486 5B; part iii), yielding $p < .0005$.

Overall the observed pattern of inter vs. intra-subject Dice overlap provided strong evidence supporting the presence of considerable variability in the spatial distribution of individual digit representations across participants, contrasted with consistency within participants over time.

Additional features of cortical digit maps

Measures of shared cortical territory between different digit representations were calculated at each time point (Figure 6). The inter-subject average matrix reveals previously established features of SI digit representations, with higher overlap in digit pairs such as D4 and D5 and low overlap between D2 and D3 (Figure 6A), consistent with patterns of daily usage (Ejaz et al., 2015). The similarity of cortical overlap patterns for each participant and time point (Figure 6B) was assessed using a ranked Mantel test. An intra-subject value was derived for each participant from the average of matrix comparisons within subject but over time. An inter-subject value was derived for each participant from the average of matrix comparisons between that subject and all other subjects for a given time point; this was repeated for each time point and the results were averaged. Comparison of the intra- versus inter-subject Mantel test values revealed greater similarity of values within a given subject compared with across different subjects: paired sample t-test, $t(8)= -7.17$, $p< .0005$.

Measures of peak-to-peak distance for adjacent digit representations were calculated at each time point. These measurements are provided in full in table 3. The intra-subject consistency in these measured was quantified using Cronbach's

α, which returned the following values: D2-D3: 0.9714, D3-D4: 0.8526, and D4-D5: 0.8422. These measures support a high degree of consistency across the observed digit maps over time.

Multiple digit maps across SI

To reveal additional maps previously reported in SI with weaker digit selectivity (Kaas et al., 1979; Pons et al., 1985; Huffman and Krubitzer, 2001), an all-session average phase-encoding map was produced for each participant and resampled into a common space (FDR thresholding, α=0.01). Additional maps were seen in a subset of participants. A more anterior map was observed in some individuals (Figure 7B,C,E,F), and a more posterior map (Figure 7G,H) in others, both within SI (see Discussion for further information regarding SI subdivisions).

Strong concordance between phase-encoding and block design activation

In order to validate finger selectivity identified using the phase-encoding task, concordance with independently derived sets of digit map data from a GLM analysis of the block task was assessed. The normalised beta values from the block task GLM contrasts comparing each digit to rest (e.g. D2 > rest) were extracted at the peak voxel of each phase-encoding derived digit representation (Figure 8). These values were averaged for each digit across the three scan sessions for each participant.

A two-way repeated measures ANOVA was performed to assess the agreement of the two mapping methods, with one factor of phase-encoding digit representation (D2-D5) and one factor of block design digit representation (D2-

D5). There was a significant interaction between phase-encoding digit representation and block design digit representation on the normalised beta value: $F(9,72) = 69.15$, $p < .001$, sphericity assumed. Post-hoc paired samples t-tests demonstrated a significantly stronger relationship between the phase-encoding and block design digit representations for 'same' digits compared with 'different' digits (all $p < .0005$, uncorrected). For example, the peak voxel for phase-encoding D2 has larger beta value for the D2 > rest block task contrast compared with other digit contrasts from the block design (e.g. the D4 > rest GLM contrast). These results indicate an agreement between the two mapping methods: the peak voxel from the phase-encoding-derived map of a given digit shows a maximal normalised beta value for the GLM contrast specific to the same digit.

Discussion

In the present study we report highly reproducible maps of fine grain digit somatotopy in SI at the level of individual participants, as demonstrated in all nine participants under study (Figure 3/4). These maps were reproducible across up to a four-week interval (Figure 5A). The consistency across this interval is particularly striking given the minimally supervised and easily implemented motor task used in this study. Unlike previously reported passive sensory stimulation paradigms used in digit mapping (Huang and Sereno, 2007; Sanchez-Panchuelo et al., 2010; Martuzzi et al., 2014; Stringer et al., 2014), the motor task applied here is more akin to everyday use of the hand.

561 The map reproducibility observed within individuals was sharply contrasted by
562 a high degree of spatial variability in these maps across different participants.
563 Despite a common ordering and progression of digits along the central sulcus
564 (Figure 3/4), the shape and relative position of these representations differed, as
565 has been shown previously in primates (Merzenich et al., 1987). We demonstrate
566 the existence of considerable inter-subject variability in the spatial distribution
567 of individual digit representations (Figure 5B; Table 3). Taken together these
568 results robustly demonstrate the presence of very stable fine-grain somatotopy
569 of the four digits under study in human SI, but also highlight the population
570 variability in such detailed functional architecture in the human brain.
571
572 *Digit maps in Brodmann area 3b and beyond*
573 Using the FDR threshold applied here (α=0.001), the maps observed at each time
574 point across all participants under study were located in a region anatomically
575 consistent with Brodmann area 3b (Figure 3/4). The presence of well-delineated
576 maps in Brodmann area 3b is well described in microelectrode mapping studies
577 of individual digits in non-human primates (Kaas et al., 1979; Merzenich et al.,
578 1987). The winner-takes-all phase-encoding approach applied herein is well
579 suited to revealing such regions of high digit selectivity. This strong digit
580 selectivity was an important feature in being able to address the question of
581 consistency in such fine-grain cortical organization.
582
583 Digit maps in Brodmann area 3a, 1 and 2 show more limited digit selectivity
584 (Kaas et al., 1979; Pons and Kaas, 1986; Huffman and Krubitzer, 2001). Although
585 it was not possible to resolve evidence for these maps at each time point (Figure

3/4), pooling phase-encoding data across the three time points under study to produce an all-session average and using a more liberal FDR threshold provided further insight (Figure 7). Some individual participants displayed very clear smaller maps anterior and posterior to that presumed to be area 3b. These maps are potentially consistent with Brodmann area 3a and Brodmann area 1/2 respectively.

Since our data does not allow us to reliably define the constituent Brodmann areas in S1 at the level of individual participants, we are unable to discuss the position of these additional maps. While atlases do provide Brodmann area boundaries, these vary considerably across individuals and accurate definition would rely on cytoarchitectural information rather than gross anatomy (Zilles and Amunts, 2010). Indeed certain subdivisions (3a/4) are challenging to definitely delineate even on the basis of cytoarchitecture (Mountcastle, 2005).

Digit map reproducibility and variability

In this study we demonstrate, both qualitatively (Figure 3/4) and quantitatively (Figure 5A), a strikingly high degree of reproducibility in digit somatotopy. Previous work at 7-tesla has reported measures of digit map reproducibility either only across different runs within a single scanning session (Stringer et al., 2011) or consistency in the relatively crude measure of centre of mass location of digit representations in subjects scanned on two occasions with variable intervals between them (Martuzzi et al., 2014). Here we were able to provide evidence for very clear reproducibility in digit maps based on the two dimensional area of digit representations on the cortical surface. This was also

supported by additional measures of reproducibility: measures of shared cortical territory of different digit representations and peak-to-peak distance between adjacent representations (Figure 6; Table 3). These same measures also highlight the variability seen across participants.

Somatosensory cortex and motor function

SI acts broadly as both a processing region for afferent sensory inputs, as well as a more central node in the redirection of incoming sensory information across the sensorimotor network (Mountcastle, 2005). The region shows highly organized reciprocal connections with primary motor cortex (M1) (Darian-Smith et al., 1993; Moore et al., 2000) and is co-activated with M1 during both active and illusory movement of the hand (Porro et al., 1996; Naito et al., 2005). Furthermore, it is increasingly clear that SI exerts a strong influence on the function of M1 (Sakamoto et al., 1987; Widener and Cheney, 1997; Vidoni et al., 2010; Platz et al., 2012; Jacobs et al., 2014).

In light of the structural and functional interplay between SI and M1, a natural sensorimotor task such as hand movement will elicit robust activation of SI. The phase-encoding paradigm applied in this study is targeted as resolving the kind of ordered smooth somatotopy reported previously in SI rather than M1 (Sanchez-Panchuelo et al., 2010; Martuzzi et al., 2014; Stringer et al., 2014). However other approaches have provided evidence for representation of specific movements or digits in different neuronal populations or cortical regions of M1, though not strictly digit somatotopy (Schieber and Hibbard, 1993; Nudo et al., 1996). Indeed, work in humans suggests motor representations may be encoded

636 in a higher dimensionality space rather than as individual body parts (Overduin
637 et al., 2012; Diedrichsen et al., 2013; Wiestler et al., 2013). However, recent work
638 combining fMRI and electrocorticography does provide evidence for some
639 ordered digit topography in M1 (Siero et al., 2014).
640
641 *Digit mapping: plasticity and disease*
642 The presence of stable but variable somatotopic maps raises the possibility of
643 investigating the factors underlying individual differences in cortical functional
644 architecture. In addition, the observation of stability in even the most fine grain
645 SI somatotopy provides a firm foundation for studies of plasticity, for example
646 using within-subject longitudinal study designs. Such work might consider the
647 potential for remapping in health and disease, building upon previous studies
648 using MEG (Braun et al., 2000; Schwenkreis et al., 2001; Candia et al., 2003;
649 Stavrinou et al., 2007). Furthermore, the reproducibility of these maps combined
650 with the short 10-minute acquisition time and simple motor paradigm, provides
651 encouraging evidence for the clinical utility of single-participant fMRI. Mapping
652 techniques could be of particular interest in presurgical planning or monitoring
653 longitudinal changes in patient populations (Hirsch et al., 2000; Yoo et al., 2005;
654 Bosnell et al., 2008; Gountouna et al., 2010).
655
656 *Phase-encoding and digit mapping*
657 We provide evidence of concordance between digit maps derived from phase-
658 encoding and more traditional block designs (Figure 8). Previous work in body
659 mapping has also demonstrated agreement between phase-encoding maps and
660 mapping results from other fMRI paradigms, including block designs (Orlov et al.,

2010; Besle et al., 2013a), event related designs (Besle et al., 2013a), and resting state functional connectivity data (Zeharia et al., 2015). The results presented here provide further compelling evidence that the phase-encoding analysis provides a meaningful method of mapping patterns of topography.

Limitations

The use of a motor task in assessing SI topography has a number of limitations. Firstly, it is not possible to isolate the exact somaesthetic sub-modality responsible for these maps, which could be induced by stimulation of cutaneous or subcutaneous receptors, or deeper proprioceptors. However, typical use of the hand recruits a combination of such receptors, as such this task represents a more naturalistic assessment of SI function than somatosensory stimulation in the absence of movement. In light of the active task applied in this study it would also be challenging to make inferences about Brodmann area somaesthetic sub-modality specificity.

Given the anatomical enslavement of certain adjacent digit pairs, it is possible that in moving certain fingers, adjacent fingers will also be moved to a lesser extent. Variability in this enslavement could contribute to the inter-subject differences reported in this study. However, given the relatively universal anatomical basis of enslavement (Yu et al., 2010), it seems unlikely that this could account for the considerable variance observed in the functional architecture of the cortex observed here. Moreover, the phenomenon of enslavement is more marked in extension rather than the flexion involved in button press tasks (Yu et al., 2010).

686

687 The coverage limitations of ultra-high resolution fMRI at 7T constrained the
688 region of interest to SI, preventing any assessment of secondary somatosensory
689 cortex or subcortical grey matter structures, where somatotopy has previously
690 been reported (Lenz and Byl, 1999; Ruben et al., 2001; Huang and Sereno, 2007).

691

692 ## Conclusions

693 This study robustly demonstrates the presence of stable digit somatotopy of four
694 digits in human SI, as well as the considerable inter-subject variability in these
695 representations. The use of fMRI to demonstrate this reproducibility at the level
696 of single participants provides a firm foundation for this non-invasive imaging
697 technique to investigate highly detailed functional organization of the human
698 brain. The mapping paradigm validated in this study has potential applications
699 both in the study of sensorimotor plasticity in the context of both learning and
700 pathological dysfunction, as well as in the clinical setting.

701

702 ## References

703 Allard T, Clark SA, Jenkins WM, Merzenich MM (1991) Reorganization of
704 somatosensory area 3b representations in adult owl monkeys after digital
705 syndactyly. J Neurophysiol 66:1048–1058.

706 Bara-Jimenez W, Catalan MJ, Hallett M, Gerloff C (1998) Abnormal
707 somatosensory homunculus in dystonia of the hand. Ann Neurol 44:828–831.

708 Baumgartner C, Doppelbauer A, Deecke L, Barth ML, Zeitlhofer J, Lindinger G,
709 Sutherling WW (1991) Neuromagnetic investigation of somatotopy of human
710 hand somatosensory cortex. Exp Brain Res 87:641–648.

711 Besle J, Sanchez-Panchuelo R-M, Bowtell R, Francis ST, Schluppeck D (2013a)
712 Single-subject fMRI mapping at 7 T of the representation of fingertips in S1: a
713 comparison of event-related and phase-encoding designs. J Neurophysiol
714 109:2293–2305.

715 Besle J, Sanchez-Panchuelo R-M, Bowtell R, Francis ST, Schluppeck D (2013b)
716 Event-related fMRI at 7T reveals overlapping cortical representations for
717 adjacent fingertips in S1 of individual subjects. Hum Brain Mapp 35:2027–
718 2043.

719 Bosnell RA et al. (2008) Reproducibility of fMRI in the clinical setting:
720 Implications for trial designs. NeuroImage 42:603–610.

721 Braun C, Wilms A, Schweizer R, Godde B, Preissl H, Birbaumer N (2000) Activity
722 patterns of human somatosensory cortex adapt dynamically to stimulus
723 properties. Neuroreport 11:2977–2980.

724 Butterworth S, Francis ST, Kelly E, McGlone F, Bowtell R, Sawle GV (2003)
725 Abnormal cortical sensory activation in dystonia: An fMRI study. Mov Disord
726 18:673–682.

727 Candia V, Wienbruch C, Elbert T, Rockstroh B, Ray W (2003) Effective behavioral
728 treatment of focal hand dystonia in musicians alters somatosensory cortical
729 organization. Proc Natl Acad Sci USA 100:7942–7946.

730 Dale AM, Fischl B, Sereno MI (1999) Cortical surface-based analysis. I.
731 Segmentation and surface reconstruction. NeuroImage 9:179–194.

732 Darian-Smith C, Darian-Smith I, Burman K, Ratcliffe N (1993) Ipsilateral cortical
733 projections to areas 3a, 3b, and 4 in the macaque monkey. J Comp Neurol
734 335:200–213.

735 Dice LR (1945) Measures of the Amount of Ecologic Association Between
736 Species. Ecology 26:297–302.

737 Diedrichsen J, Wiestler T, Ejaz N (2013) A multivariate method to determine the
738 dimensionality of neural representation from population activity.
739 NeuroImage 76:225–235.

740 Ejaz N, Hamada M, Diedrichsen J (2015) Hand use predicts the structure of
741 representations in sensorimotor cortex. Nat Neurosci 18:1034–1040.

742 Elbert T, Candia V, Altenmüller E, Rau H, Sterr A, Rockstroh B, Pantev C, Taub E
743 (1998) Alteration of digital representations in somatosensory cortex in focal
744 hand dystonia. Neuroreport 9:3571.

745 Engel SA (2012) The development and use of phase-encoded functional MRI
746 designs. NeuroImage 62:1195–1200.

747 Engel SA, Glover GH, Wandell BA (1997) Retinotopic organization in human
748 visual cortex and the spatial precision of functional MRI. Cereb Cortex 7:181–
749 192.

750 Fischl B, Liu A, Dale AM (2001) Automated manifold surgery: constructing
751 geometrically accurate and topologically correct models of the human
752 cerebral cortex. IEEE Trans Med Imaging 20:70–80.

753 Francis ST, Kelly EF, Bowtell R, Dunseath WJR, Folger SE, McGlone F (2000) fMRI
754 of the Responses to Vibratory Stimulation of Digit Tips. NeuroImage 11:188–
755 202.

756 Gelnar PA, Krauss BR, Szeverenyi NM, Apkarian AV (1998) Fingertip
757 representation in the human somatosensory cortex: an fMRI study.
758 NeuroImage 7:261–283.

759 Genovese CR, Lazar NA, Nichols T (2002) Thresholding of statistical maps in
760 functional neuroimaging using the false discovery rate. NeuroImage 15:870–
761 878.

762 Gountouna V-E, Job DE, McIntosh AM, Moorhead TWJ, Lymer GKL, Whalley HC,
763 Hall J, Waiter GD, Brennan D, McGonigle DJ, Ahearn TS, Cavanagh J, Condon B,
764 Hadley DM, Marshall I, Murray AD, Steele JD, Wardlaw JM, Lawrie SM (2010)
765 Functional Magnetic Resonance Imaging (fMRI) reproducibility and variance
766 components across visits and scanning sites with a finger tapping task.
767 NeuroImage 49:552–560.

768 Greene D, Cunningham P (2006) Practical solutions to the problem of diagonal
769 dominance in kernel document clustering. In, pp 377–384. New York, New
770 York, USA: ACM Press.

771 Greve DN, Fischl B (2009) Accurate and robust brain image alignment using
772 boundary-based registration. NeuroImage 48:63–72.

773 Hirsch J, Ruge MI, Kim KH, Correa DD, Victor JD, Relkin NR, Labar DR, Krol G,
774 Bilsky MH, Souweidane MM, DeAngelis LM, Gutin PH (2000) An integrated
775 functional magnetic resonance imaging procedure for preoperative mapping
776 of cortical areas associated with tactile, motor, language, and visual
777 functions. Neurosurgery 47:711–21–discussion721–2.

778 Huang R-S, Sereno MI (2007) Dodecapus: An MR-compatible system for
779 somatosensory stimulation. NeuroImage 34:1060–1073.

780 Huffman KJ, Krubitzer L (2001) Area 3a: topographic organization and cortical
781 connections in marmoset monkeys. Cereb Cortex 11:849–867.

782 Jacobs MF, Tsang P, Lee KGH, Asmussen MJ, Zapallow CM, Nelson AJ (2014) 30
783 Hz theta-burst stimulation over primary somatosensory cortex modulates
784 corticospinal output to the hand. Brain Stimulation 7:269–274.

785 Jenkinson M, Bannister PR, Brady M, Smith S (2002) Improved Optimization for
786 the Robust and Accurate Linear Registration and Motion Correction of Brain
787 Images. NeuroImage 17:825–841.

788 Jenkinson M, Beckmann CF, Behrens TEJ, Woolrich MW, Smith SM (2012) FSL.
789 NeuroImage 62:782–790.

790 Jenkinson M, Smith S (2001) A global optimisation method for robust affine
791 registration of brain images. Med Image Anal 5:143–156.

792 Kaas JH, Nelson RJ, Sur M, Lin C-S, Merzenich MM (1979) Multiple
793 representations of the body within the primary somatosensory cortex of
794 primates. Science 204:521–523.

795 Kurth R, Villringer K, Mackert BM, Schwiemann J, Braun J, Curio G, Villringer A,
796 Wolf KJ (1998) fMRI assessment of somatotopy in human Brodmann area 3b
797 by electrical finger stimulation. Neuroreport 9:207–212.

798 Lenz FA, Byl NN (1999) Reorganization in the Cutaneous Core of the Human
799 Thalamic Principal Somatic Sensory Nucleus (Ventral Caudal) in Patients
800 With Dystonia. J Neurophysiol 82:3204–3212.

801 Mancini F, Haggard P, Iannetti GD, Longo MR, Sereno MI (2012) Fine-grained
802 nociceptive maps in primary somatosensory cortex. J Neurosci 32:17155–
803 17162.

804 Mantel N (1967) The detection of disease clustering and a generalized regression
805 approach. Cancer Res 27:209–220.

806 Marcus DS, Harwell J, Olsen T, Hodge M, Glasser MF, Prior F, Jenkinson M,
807 Laumann T, Curtiss SW, Van Essen DC (2011) Informatics and data mining
808 tools and strategies for the human connectome project. Front Neuroinform
809 5:4.

810 Martuzzi R, van der Zwaag W, Farthouat J, Gruetter R, Blanke O (2014) Human
811 finger somatotopy in areas 3b, 1, and 2: a 7T fMRI study using a natural
812 stimulus. Hum Brain Mapp 35:213–226.

813 Merzenich MM, Nelson RJR, Kaas JH, Stryker MPM, Jenkins WMW, Zook JM,
814 Cynader MS, Schoppmann AA (1987) Variability in hand surface
815 representations in areas 3b and 1 in adult owl and squirrel monkeys. J Comp
816 Neurol 258:281–296.

817 Meunier S, Garnero L, Ducorps A, Mazi res L, Leh ricy SP, T zenas Du Montcel S,
818 Renault B, Vidailhet M (2001) Human brain mapping in dystonia reveals both
819 endophenotypic traits and adaptive reorganization. Ann Neurol 50:521–527.

820 Moore CI, Stern CE, Corkin S, Fischl B, Gray AC, Rosen BR, Dale AM (2000)
821 Segregation of somatosensory activation in the human rolandic cortex using
822 fMRI. J Neurophysiol 84:558–569.

823 Moulton EA, Pendse G, Morris S, Aiello-Lammens M, Becerra L, Borsook D (2009)
824 Segmentally arranged somatotopy within the face representation of human
825 primary somatosensory cortex. Hum Brain Mapp 30:757–765.

826 Mountcastle VB (2005) The Sensory Hand. Harvard University Press.

827 Naito E, Roland PE, Grefkes C, Choi HJ, Eickhoff SB, Geyer S, Zilles K, Ehrsson HH
828 (2005) Dominance of the right hemisphere and role of area 2 in human
829 kinesthesia. J Neurophysiol 93:1020–1034.

830 Nelson AJ, Blake DT, Chen R (2009) Digit-specific aberrations in the primary
831 somatosensory cortex in Writer's cramp. Ann Neurol 66:146–154.

832 Nelson AJ, Chen R (2008) Digit somatotopy within cortical areas of the
833 postcentral gyrus in humans. Cerebral Cortex 18:2341–2351.

834 Nudo RJ, Milliken GW, Jenkins WM, Merzenich MM (1996) Use-dependent
835 alterations of movement representations in primary motor cortex of adult
836 squirrel monkeys. J Neurosci 16:785–807.

837 Oldfield RC (1971) The assessment and analysis of handedness: the Edinburgh
838 inventory. Neuropsychologia 9:97–113.

839 Orlov T, Makin TR, Zohary E (2010) Topographic Representation of the Human
840 Body in the Occipitotemporal Cortex. Neuron 68:586–600.

841 Overduin SA, d'Avella A, Carmena JM, Bizzi E (2012) Microstimulation Activates a
842 Handful of Muscle Synergies. Neuron 76:1071–1077.

843 Overduin SA, Servos P (2004) Distributed digit somatotopy in primary
844 somatosensory cortex. NeuroImage 23:462–472.

845 Penfield W, Boldrey E (1937) Somatic motor and sensory representation in the
846 cerebral cortex of man as studied by electrical stimulation. Brain 60:389–
847 443.

848 Platz T, Roschka S, Christel MI, Duecker F, Rothwell JC, Sack AT, Sack A (2012)
849 Early stages of motor skill learning and the specific relevance of the cortical
850 motor system--a combined behavioural training and θ burst TMS study.
851 Restor Neurol Neurosci 30:199–211.

852 Pons TP, Garraghty PE, Cusick CG, Kaas JH (1985) The somatotopic organization
853 of area 2 in macaque monkeys. J Comp Neurol 241:445–466.

854 Pons TP, Kaas JH (1986) Corticocortical connections of area 2 of somatosensory
855 cortex in macaque monkeys: a correlative anatomical and
856 electrophysiological study. J Comp Neurol 248:313–335.

857 Porro CA, Francescato MP, Cettolo V, Diamond ME, Baraldi P, Zuiani C, Bazzocchi
858 M, di Prampero PE (1996) Primary motor and sensory cortex activation
859 during motor performance and motor imagery: a functional magnetic
860 resonance imaging study. J Neurosci 16:7688–7698.

861 Postelnicu G, Zollei L, Fischl B (2009) Combined volumetric and surface
862 registration. IEEE Trans Med Imaging 28:508–522.

863 Ruben J, Schwiemann J, Deuchert M, Meyer R, Krause T, Curio G, Villringer K,
864 Kurth R, Villringer A (2001) Somatotopic organization of human secondary
865 somatosensory cortex. Cereb Cortex 11:463–473.

866 Sakamoto T, Porter LL, Asanuma H (1987) Long-lasting potentiation of synaptic

potentials in the motor cortex produced by stimulation of the sensory cortex in the cat: a basis of motor learning. Brain Res 413:360–364.

Sanchez-Panchuelo RM, Besle J, Beckett A, Bowtell R, Schluppeck D, Francis ST (2012) Within-Digit Functional Parcellation of Brodmann Areas of the Human Primary Somatosensory Cortex Using Functional Magnetic Resonance Imaging at 7 Tesla. J Neurosci 32:15815–15822.

Sanchez-Panchuelo RM, Francis ST, Bowtell R, Schluppeck D (2010) Mapping human somatosensory cortex in individual subjects with 7T functional MRI. J Neurophysiol 103:2544–2556.

Schieber MH, Hibbard LS (1993) How somatotopic is the motor cortex hand area? Science 261:489–492.

Schweizer R, Voit D, Frahm J (2008) Finger representations in human primary somatosensory cortex as revealed by high-resolution functional MRI of tactile stimulation. NeuroImage 42:28–35.

Schwenkreis P, Pleger B, Höffken O, Malin JP, Tegenthoff M (2001) Repetitive training of a synchronised movement induces short-term plastic changes in the human primary somatosensory cortex. Neurosci Lett 312:99–102.

Sereno MI, Huang R-S (2006) A human parietal face area contains aligned head-centered visual and tactile maps. Nat Neurosci 9:1337–1343.

Siero JCW, Hermes D, Hoogduin H, Luijten PR, Ramsey NF, Petridou N (2014) BOLD matches neuronal activity at the mm scale: a combined 7T fMRI and ECoG study in human sensorimotor cortex. NeuroImage 101:177–184.

Smith SM (2002) Fast robust automated brain extraction. Hum Brain Mapp 17:143–155.

Smith SM, Jenkinson M, Woolrich MW, Beckmann CF, Behrens TEJ, Johansen-Berg H, Bannister PR, De Luca M, Drobnjak I, Flitney DE, Niazy RK, Saunders J, Vickers J, Zhang Y, De Stefano N, Brady JM, Matthews PM (2004) Advances in functional and structural MR image analysis and implementation as FSL. NeuroImage 23:S208–S219.

Stavrinou ML, Penna Della S, Pizzella V, Torquati K, Cianflone F, Franciotti R, Bezerianos A, Romani GL, Rossini PM (2007) Temporal dynamics of plastic changes in human primary somatosensory cortex after finger webbing. Cereb Cortex 17:2134–2142.

Stringer EA, Chen LM, Friedman RM, Gatenby JC, Gore JC (2011) Differentiation of somatosensory cortices by high-resolution fMRI at 7 T. NeuroImage 54:1012–1020.

Stringer EA, Qiao P-G, Friedman RM, Holroyd L, Newton AT, Gore JC, Min Chen L (2014) Distinct fine-scale fMRI activation patterns of contra- and ipsilateral somatosensory areas 3b and 1 in humans. Hum Brain Mapp 35:4841–4857.

van der Kouwe AJW, Benner T, Salat DH, Fischl B (2008) Brain morphometry with multiecho MPRAGE. NeuroImage 40:559–569.

van der Zwaag W, Kusters R, Magill A, Gruetter R, Martuzzi R, Blanke O, Marques JP (2013) Digit somatotopy in the human cerebellum: A 7T fMRI study. NeuroImage 67:1–9.

Vidoni ED, Acerra NE, Dao E, Meehan SK, Boyd LA (2010) Role of the primary somatosensory cortex in motor learning: An rTMS study. Neurobiology of Learning and Memory 93:532–539.

Vidyasagar R, Folger SE, Parkes LM (2014) Re-wiring the brain: increased functional connectivity within primary somatosensory cortex following synchronous co-activation. NeuroImage 92:19–26.

Vidyasagar R, Parkes LM (2011) Reproducibility of functional MRI localization within the human somatosensory cortex. J Magn Reson Imaging 34:1439–1444.

Walter H, Kristeva R, Knorr U, Schlaug G, Huang Y, Steinmetz H, Nebeling B, Herzog H, Seitz RJ (1992) Individual somatotopy of primary sensorimotor cortex revealed by intermodal matching of MEG, PET, and MRI. Brain Topogr 5:183–187.

Wandell BA, Dumoulin SO, Brewer AA (2007) Visual field maps in human cortex. Neuron 56:366–383.

Widener GL, Cheney PD (1997) Effects on muscle activity from microstimuli applied to somatosensory and motor cortex during voluntary movement in the monkey. J Neurophysiol 77:2446–2465.

Wiestler T, Diedrichsen J, Culham JC (2013) Skill learning strengthens cortical representations of motor sequences. eLife 2.

Woolrich MW, Jbabdi S, Patenaude B, Chappell M, Makni S, Behrens TEJ, Beckmann CF, Jenkinson M, Smith SM (2009) Bayesian analysis of neuroimaging data in FSL. NeuroImage 45:S173–S186.

Yau JM, Connor CE, Hsiao SS (2013) Representation of tactile curvature in macaque somatosensory area 2. J Neurophysiol 109:2999–3012.

Yoo S-S, Wei X, Dickey CC, Guttmann CRG, Panych LP (2005) Long-term reproducibility analysis of fMRI using hand motor task. Int J Neurosci 115:55–77.

Yousry TA, Schmid UD, Alkadhi H, Schmidt D, Peraud A, Buettner A, Winkler P (1997) Localization of the motor hand area to a knob on the precentral gyrus. A new landmark. Brain 120 (Pt 1):141–157.

Yu WS, van Duinen H, Gandevia SC (2010) Limits to the Control of the Human Thumb and Fingers in Flexion and Extension. J Neurophysiol 103:278–289.

944 Zarzecki P, Witte S, Smits E, Gordon DC, Kirchberger P, Rasmusson DD (1993)
945 Synaptic mechanisms of cortical representational plasticity: somatosensory
946 and corticocortical EPSPs in reorganized raccoon SI cortex. J Neurophysiol
947 69:1422–1432.

948 Zeharia N, Hertz U, Flash T, Amedi A (2015) New Whole-Body Sensory-Motor
949 Gradients Revealed Using Phase-Locked Analysis and Verified Using
950 Multivoxel Pattern Analysis and Functional Connectivity. Journal of
951 Neuroscience 35:2845–2859.

952 Zilles K, Amunts K (2010) Centenary of Brodmann's map--conception and fate.
953 Multiple values selected 11:139–145.

954

955

Figure 1

Figure 1: Overview of phase-encoding digit mapping task and analysis

(A) The phase-encoding paradigm: 8 x 32-second cycles of continuous button presses at 1Hz. Each 32-second cycle consists of four 8-second blocks, with each block cycling through either D2-D5 (forward) or D5-D2 (backward). (B) BOLD timecourses from individual voxels (one timecourse shown) cross-correlated against reference models (8-second 'on', 24-seconds 'off'), shifted iteratively by a number of lags to capture activation throughout the movement cycles. (C) Plotting cross-correlation of each voxel's timecourse as a function of lag reveals peak cross-correlation at a given lag. Four different voxels shown, each with a cross-correlation peaking in lags corresponding to different digits. (D) *r*-values for each voxel averaged across lags assigned to specific digits. Resulting digit *r*-value maps for forward and backwards cycled are also averaged to yield voxel-wise *r*-value maps for each digit for one subject/timepoint (thresholded maps displayed).

Figure 2

Figure 2: Phase-encoding digit maps from a single participant and timepoint

(A) Digit maps in BOLD EPI volumetric space across five adjacent transverse slices (z: 11-15); FDR threshold (α=0.001). Digit 2: pink, digit 3: orange, digit 4: green, digit 5: blue. R: right, L: lateral, M: medial. (B) Post-hoc analysis of BOLD signal from individual digit representations in this participant. (C/D) Surface projection of digit maps shown on the inflated pial surface (black: sulcal pattern). Red highlighted region (C: inset) indicates coverage of BOLD EPI task fMRI data partial field of view. No masking has been applied within the acquisition field of view.

Figure 3

Figure 3: Temporal reproducibility of phase-encoding digit maps within-participant.

Comparison of phase-encoding digit representations at three scan timepoints for three participants. Although there is a high degree of between-subject variability (as shown by the large differences between rows), there is very littlewithin-subject variability over time (demonstrated by the small differences across each row). Cortical maps shown on the inflated pial surface with the sulcal pattern in black (positive curvature). Zoomed panels are centred on the hand knob of the central sulcus. All digit maps are subject to FDR thresholding (α=0.001); full details of thresholds and maxima for each time point provided in table 2; colour bars represent range from zero to maximum.

Figure 4

Figure 4: Temporal reproducibility of phase-encoding digit maps within-participant (continued)

Comparison of phase-encoding digit representations at three scan timepoints continued from figure 4 for remaining participants. All digit maps are subject to FDR thresholding (α=0.001); full details of thresholds and maxima for each time point provided in table 2.

Figure 5

Figure 5: Quantifying intra-subject reproducibility and inter-subject variability in phase-encoding digit maps

(A i-iii) Dice coefficients demonstrate a clear pattern of reproducibility for maps of homologous digits across the three timepoints under study compared with first order and second/third order neighbours. (A iv) Dice coefficients for homologous digits were greater than the equivalent value between non-homologous digit pairings: one-way repeated measures ANOVA: significant main effect of digit pairing category (homologous, first order neighour, second/third order neighbour). **: Post hoc analysis (Bonferroni adjusted): p <.0005. (B i) Dice coefficients comparing all combinations of individual digit representations across different participants (after accounting for differences in digit map size) across 0 hour and +/- 4 week timepoints. (B ii) Patterns in each digit pair sub-matrix were summarised by the matrix dominance ratio (Mdr; Equation 2) Mdr > 1 suggests greater intra-subject overlap in digit representations; Mdr < 1 implies greater inter-subject overlap in digit representations. For 'same' pairings (e.g. D2-D2) a pattern of high overlap was seen intra-subject (B i: submatrix diagonals), contrasted lower overlap values for comparisons inter-subject (B i: submatrix off-diagonals). For 'different' pairings (e.g. D2-D4) no such pattern was observed, suggesting intra-subject consistency is driven by reproducibility of the spatial patterns for the same digits over time. (B iii) Calculation of the overall Mdr (from B ii) was subjected to bootstrap resampling (50,000 iterations) to account for the likelihood of observing these dominance ratios by chance. Bootstrapping returned p < .0005 for the observed value of overall Mdr, consistent with the notion of inter-subject variability in fine grain digit representations.

Figure 6

Figure 6: Patterns of overlap between different digit representations
Soft-edged phase-encoding digit maps provide information regarding shared cortical territory of different digit representations. (A) Average measures of cortical overlap between different digit representations across all subjects and time points reveal pattern of greater shared territory across functionally coupled digits: the relative independence of D2, with increasing levels of cortical overlap between more synergistic D3/D4 and D4/D5. (B) Cortical overlap matrices for

individual participants and time points; ranked Mantel test statistics were used to compare matrices. Intra-subject comparisons: average Mantel test statistic for intra-subject comparisons across the three time points. Inter-subject comparisons: average of the Mantel test statistic calculated between each participant at a given time point and all other participants at that time point; calculated for each time point and averaged. (C) Comparison of the intra- versus inter-subject Mantel test statistics revealed greater similarity of values within a given subject compared with across different subjects: paired sample t-test, **: p <.0005.

Figure 7

Figure 7: Resolving additional digit maps within SI.

An all-session average phase encoding map was produced for each participant and resampled into a common space (FDR thresholding, α=0.01). Additional maps were seen in a subset of participants. A more anterior map was observed (Arrowhead: B,C,E,F) in some individuals, and a more posterior map (Arrowheads: G,H) in others, both within SI. In the remaining participants (A, D, I) no clear evidence for additional maps was found.

Figure 8

Figure 8: Validation of phase-encoding digit maps using block design data

Beta values from the block design task fMRI data were extracted for each GLM contrast (digit > rest) at the peak voxels of the phase-encoding digit representations (D2-D5). This process was repeated for each of the three scans to derive average values for each participant. For each phase-encoding digit representation the beta value of the homologous GLM contrast (e.g. D2 phase-encoding vs. D2 > rest GLM contrast), was significantly greater than for non-homologous GLM contrasts (e.g. D2 phase-encoding vs. D4 > rest GLM contrast). RM-ANOVA: significant interaction between phase-encoding digit representation and the digit contrast of the block design GLM on the normalised beta value. ** Post-hoc t-test p <.0005 (uncorrected).

Table 1

	Age	Gender	Handedness	Laterality index	Peak relative head motion (mm)
1	35	F	R	+78	0.20
2	33	M	R	+84	0.13
3	28	M	R	+82	0.32
4	25	M	R	+63	0.26
5	20	F	R	+86	0.35
6	30	F	R	+100	0.81
7	23	F	R	+92	0.20
8	40	M	R	+87	0.41
9	23	M	R	+80	0.53
10	29	F	R	+79	1.25
11	30	F	R	+100	2.65
12	24	M	R	+100	0.54
13	33	M	R	+96	4.11

Table 1: Participant demographic information

Participant demographics for the thirteen participants recruited to this study. F: female, M: male, R: right-handed. Laterality index calculated using Edinburgh Handedness Score (Oldfield *et al.* 1971).

Table 2

	0 hour				+24 hours				+/- 4 weeks			
	D2	*D3*	*D4*	*D5*	*D2*	*D3*	*D4*	*D5*	*D2*	*D3*	*D4*	*D5*
1	5.17 (7.97)	4.17 (10.6)	3.93 (5.87)	4.25 (7.62)	6.16 (9.38)	4.82 (8.13)	4.80 (10.1)	6.28 (11.4)	5.71 (10.1)	4.73 (9.26)	5.78 (11.7)	6.25 (11.2)
2	3.91 (6.53)	2.87 (6.83)	3.96 (5.46)	4.53 (9.32)	5.22 (6.91)	3.07 (5.42)	4.68 (6.63)	4.53 (7.76)	5.19 (8.98)	3.11 (5.93)	5.26 (7.44)	5.48 (8.18)
3	6.21 (9.38)	3.02 (10.7)	4.09 (12.9)	6.85 (9.11)	5.75 (10.6)	4.80 (8.94)	5.02 (12.7)	5.81 (7.53)	6.40 (11.9)	5.45 (8.84)	7.27 (12.3)	6.32 (8.39)
4	5.79 (9.79)	4.90 (8.01)	5.79 (8.91)	3.22 (7.27)	4.83 (7.88)	3.49 (6.75)	5.05 (7.98)	4.16 (6.43)	5.93 (9.47)	3.38 (6.21)	5.52 (9.14)	3.78 (6.73)
5	5.16 (7.90)	4.89 (10.1)	5.71 (8.19)	4.98 (8.02)	5.76 (8.16)	5.53 (8.66)	6.53 (8.22)	3.46 (6.72)	5.69 (8.04)	3.80 (7.02)	3.28 (6.47)	3.43 (5.70)
6	3.02 (5.30)	3.49 (5.86)	3.04 (6.24)	3.52 (6.50)	3.30 (4.60)	3.46 (5.64)	4.97 (6.52)	2.92 (4.20)	2.90 (4.80)	3.21 (9.90)	3.43 (6.41)	3.14 (5.72)
7	4.57 (6.71)	4.46 (6.13)	4.79 (7.78)	3.70 (4.90)	4.04 (5.73)	3.63 (5.63)	3.68 (5.48)	4.99 (7.06)	4.60 (6.31)	3.15 (7.08)	4.50 (7.48)	3.73 (5.11)
8	4.10 (7.99)	4.12 (13.4)	5.57 (7.96)	5.14 (8.28)	4.91 (11.2)	5.97 (14.0)	4.82 (8.58)	6.51 (9.46)	4.86 (9.89)	3.14 (8.10)	5.78 (8.87)	5.85 (10.9)
9	5.48 (8.64)	4.28 (10.5)	7.20 (9.50)	4.77 (6.03)	4.27 (9.61)	2.97 (6.01)	3.14 (9.65)	5.39 (7.20)	5.11 (8.29)	4.13 (5.26)	6.63 (10.0)	5.05 (7.46)

Table 2: FDR thresholds for single-participant digit maps

FDR thresholds (maxima in parentheses) for z-statistic phase-encoding derived digit maps for individual participants shown in Figures 3 and 4 across the three timepoints under study. FDR: false discovery rate (α=0.001). A two-way repeated measures ANOVA was performed to assess for systematic differences in FDR-defined thresholds, with one factor of digit (D2-D5) and one factor of session (0 hour, +24 hour, +/- 4 weeks). There was no significant main effect of session on FDR threshold: $F(2,16) = 0.218$, $p=0.806$, sphericity assumed.

Table 3

	Digit 2-3			Digit 3-4			Digit 4-5		
	0 hour	+24 hours	+/-4 weeks	0 hour	+ 24 hours	+/- 4 weeks	0 hour	+ 24 hours	+/- 4 weeks
1	13.56	12.53	10.53	3.38	3.99	3.61	5.82	2.75	3.55
2	15.48	14.83	15.88	8.00	4.04	3.89	8.67	11.33	10.43
3	5.45	5.14	5.16	7.35	5.19	5.56	5.51	4.67	8.13
4	14.41	16.65	16.49	4.13	3.20	3.24	4.20	11.93	11.82
5	3.48	2.26	6.11	9.11	10.56	8.65	5.06	4.66	5.66
6	13.64	9.72	13.50	5.65	6.40	12.14	6.54	5.81	5.79
7	4.62	3.19	4.62	10.64	16.21	10.64	12.37	11.09	16.87
8	10.99	11.68	9.07	6.66	5.18	5.90	4.25	7.40	4.25
9	10.51	10.32	11.03	10.55	12.10	8.63	4.32	4.85	8.00

Table 3: Peak-to-peak distances for single participant digit maps across sessions

Peak-to-peak distances (mm) derived from phase-encoding digit maps.

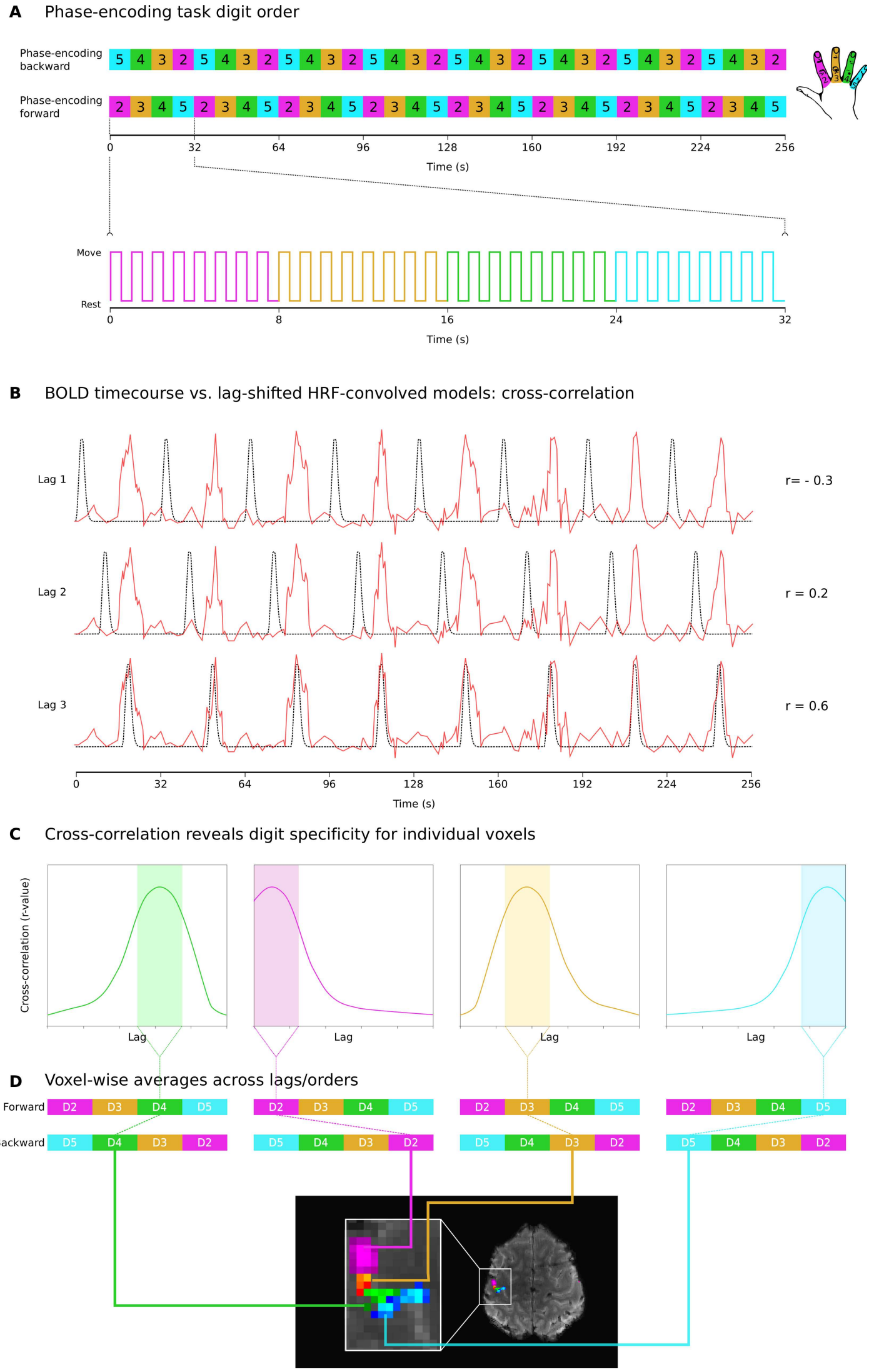
A
Phase-encoding task digit order
Phase-encoding backward
5 4 3 2 5 4 3 2 5 4 3 2 5 4 3 2 5 4 3 2 5 4 3 2 5 4 3 2 5 4 3 2
Phase-encoding forward
2 3 4 5 2 3 4 5 2 3 4 5 2 3 4 5 2 3 4 5 2 3 4 5 2 3 4 5 2 3 4 5
0 32 64 96 128 160 192 224 256
Time (s)
Move
Rest
0 8 16 24 32
Time (s)
B
BOLD timecourse vs. lag-shifted HRF-convolved models: cross-correlation
Lag 1
r= - 0.3
Lag 2
r = 0.2
Lag 3
r = 0.6
0 32 64 96 128 160 192 224 256
Time (s)
C
Cross-correlation reveals digit specificity for individual voxels
Cross-correlation (r-value)
Lag
Lag
Lag
Lag
D
Voxel-wise averages across lags/orders
Forward
D2 D3 D4 D5
Backward
D5 D4 D3 D2

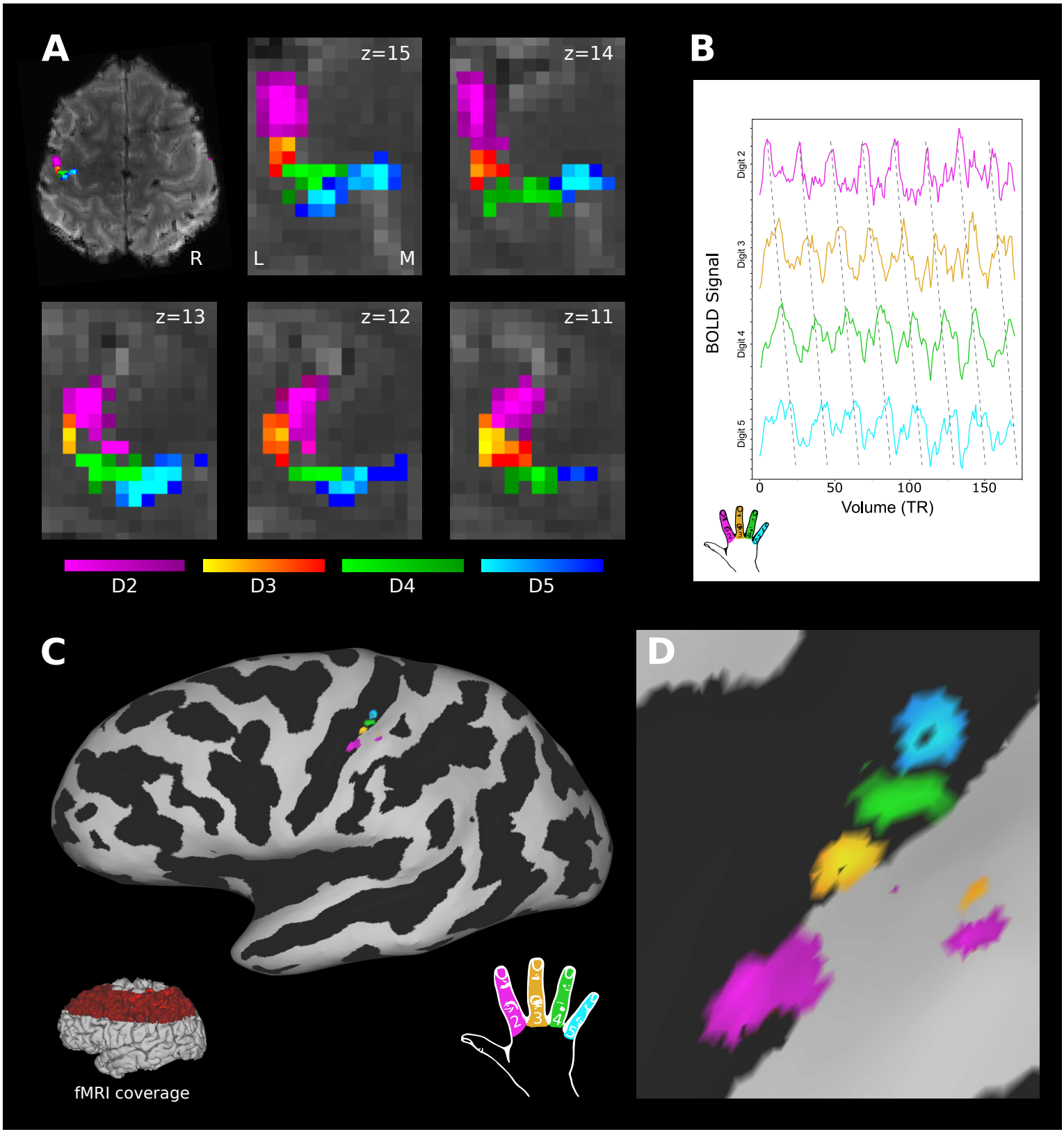
A
z=15
z=14
z=13
z=12
z=11
R
L
M
D2
D3
D4
D5
B
BOLD Signal
Digit 2
Digit 3
Digit 4
Digit 5
0
50
100
150
Volume (TR)
C
fMRI coverage
D

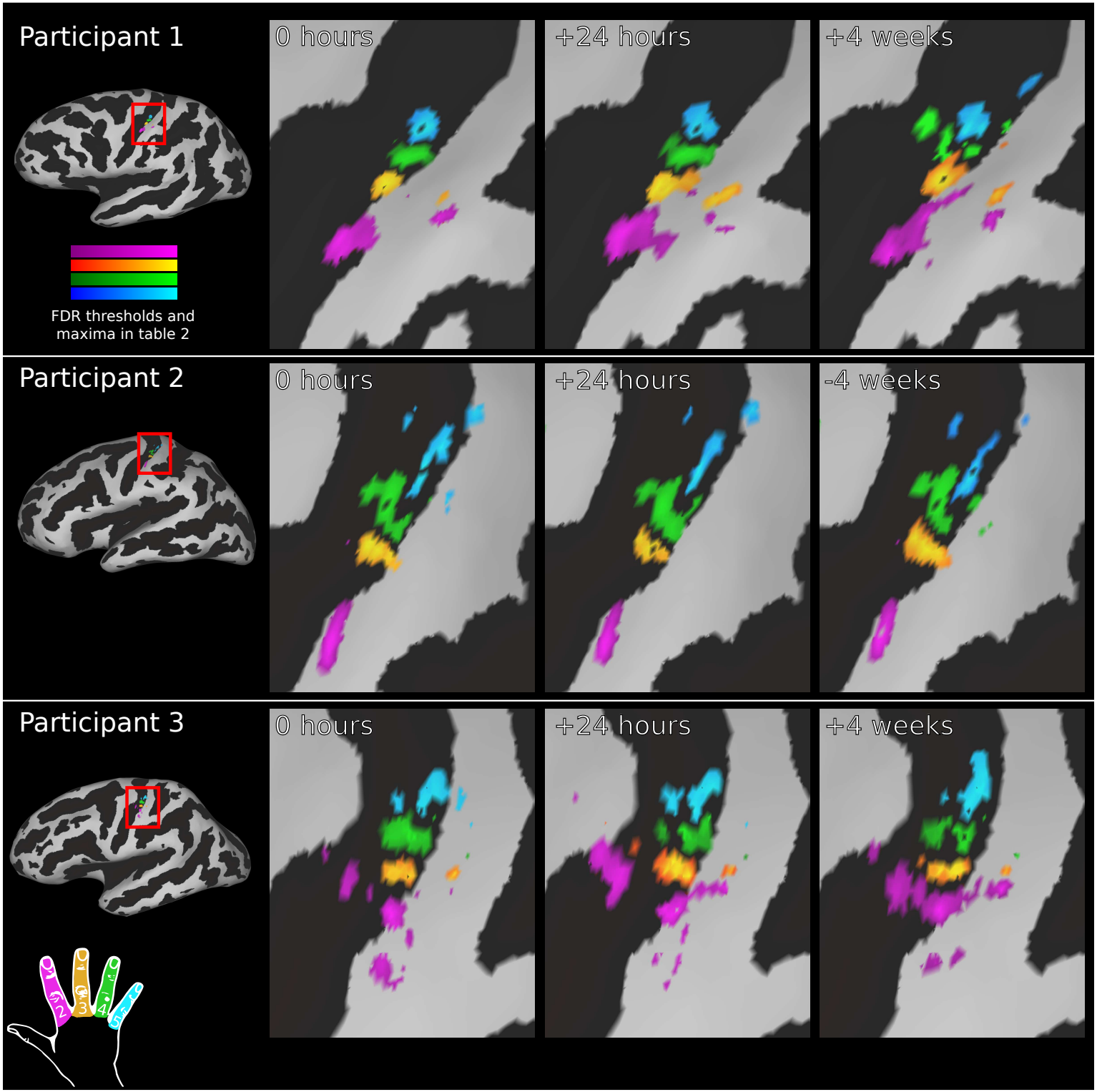
Participant 1
0 hours
+24 hours
+4 weeks
FDR thresholds and
maxima in table 2
Participant 2
0 hours
+24 hours
-4 weeks
Participant 3
0 hours
+24 hours
+4 weeks

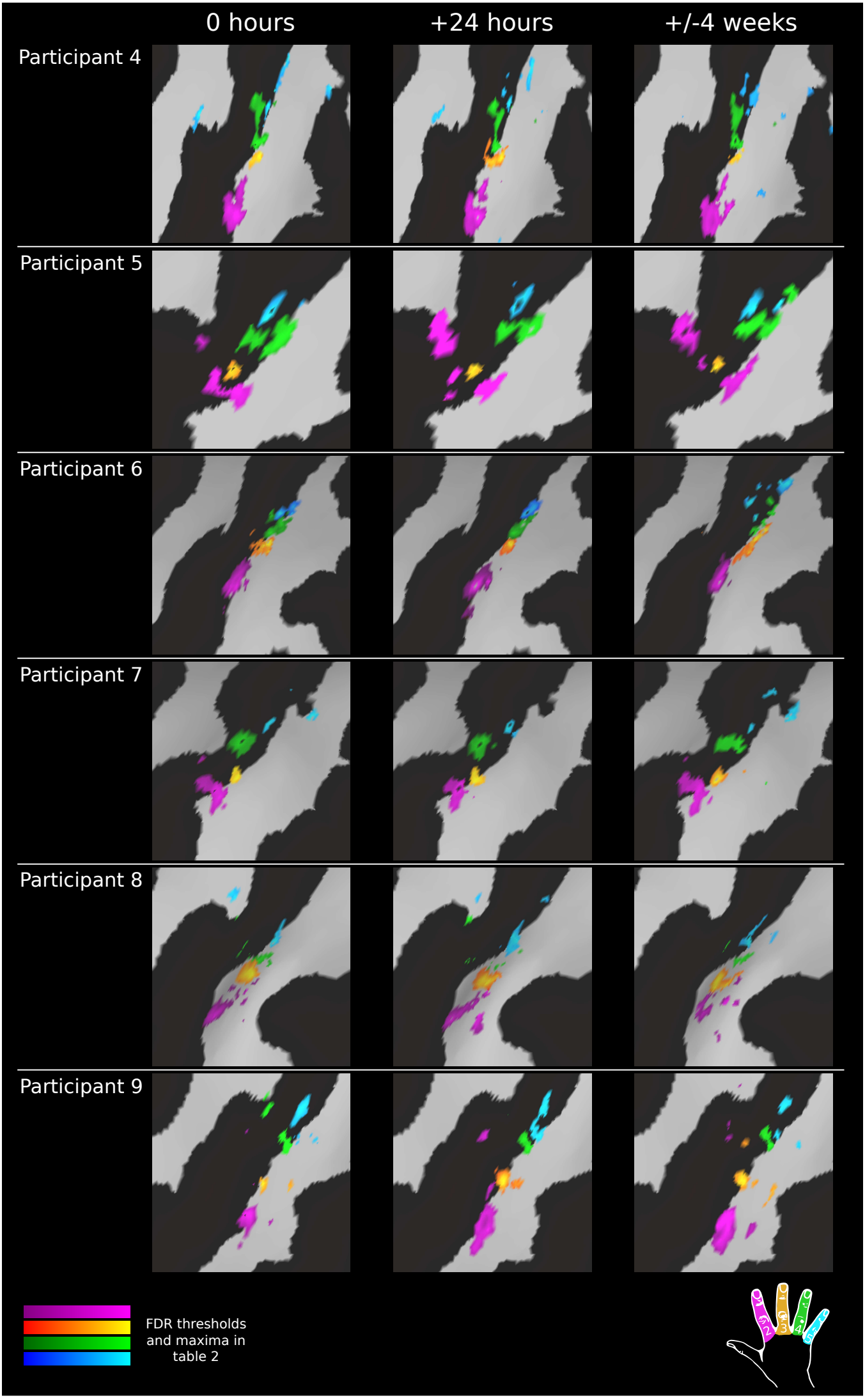
0 hours
+24 hours
+/-4 weeks
Participant 4
Participant 5
Participant 6
Participant 7
Participant 8
Participant 9
FDR thresholds and maxima in table 2

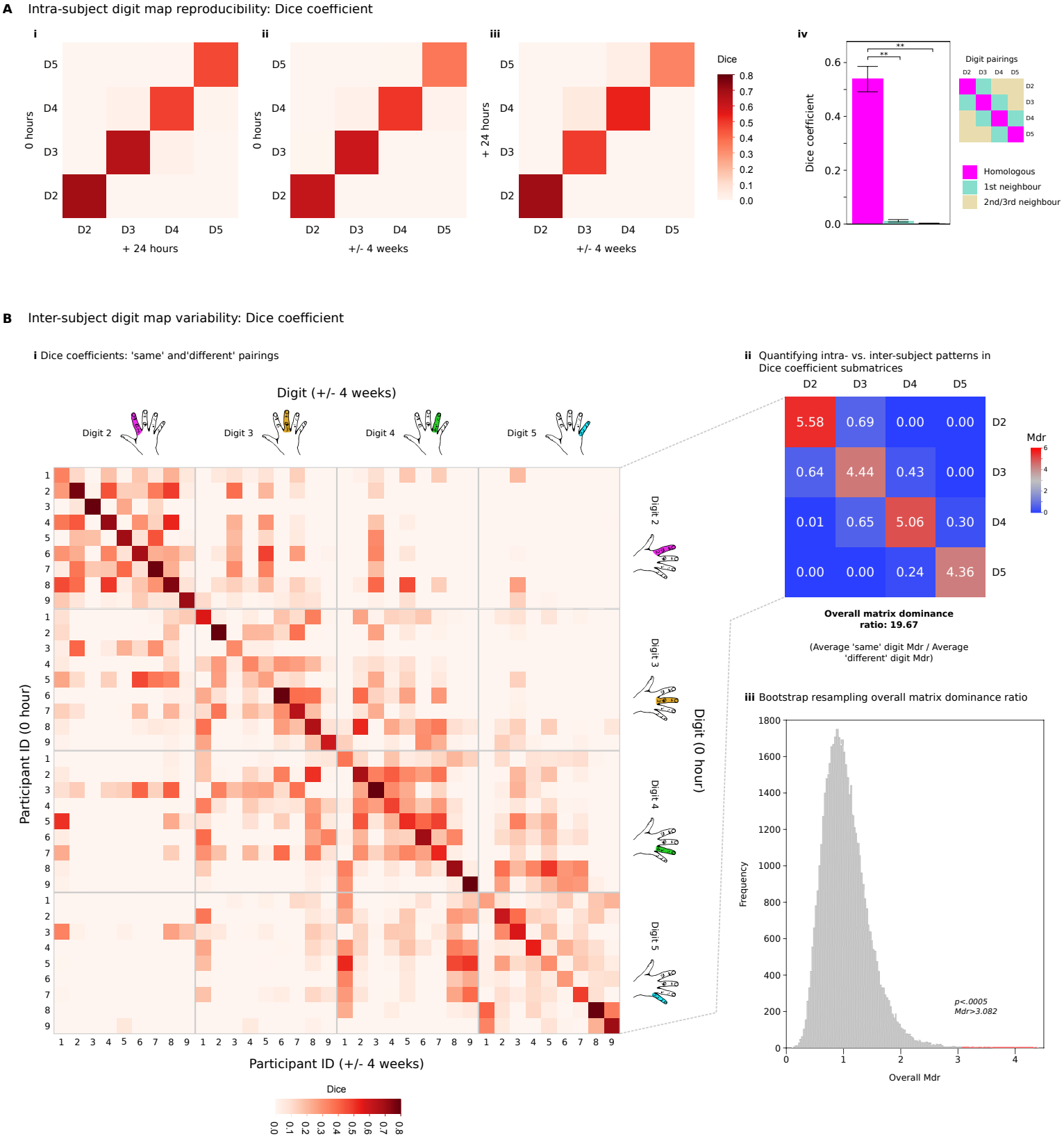
A Intra-subject digit map reproducibility: Dice coefficient
i
ii
iii
iv
0 hours
+ 24 hours
+/- 4 weeks
D2
D3
D4
D5
Dice
Dice coefficient
Digit pairings
Homologous
1st neighbour
2nd/3rd neighbour
B Inter-subject digit map variability: Dice coefficient
i Dice coefficients: 'same' and'different' pairings
Digit (+/- 4 weeks)
Digit 2
Digit 3
Digit 4
Digit 5
Participant ID (0 hour)
Participant ID (+/- 4 weeks)
Digit (0 hour)
ii Quantifying intra- vs. inter-subject patterns in Dice coefficient submatrices
5.58 0.69 0.00 0.00
0.64 4.44 0.43 0.00
0.01 0.65 5.06 0.30
0.00 0.00 0.24 4.36
Mdr
Overall matrix dominance ratio: 19.67
(Average 'same' digit Mdr / Average 'different' digit Mdr)
iii Bootstrap resampling overall matrix dominance ratio
Frequency
Overall Mdr
p<.0005
Mdr>3.082

A Overlap of different digit representations: all time point inter-subject average

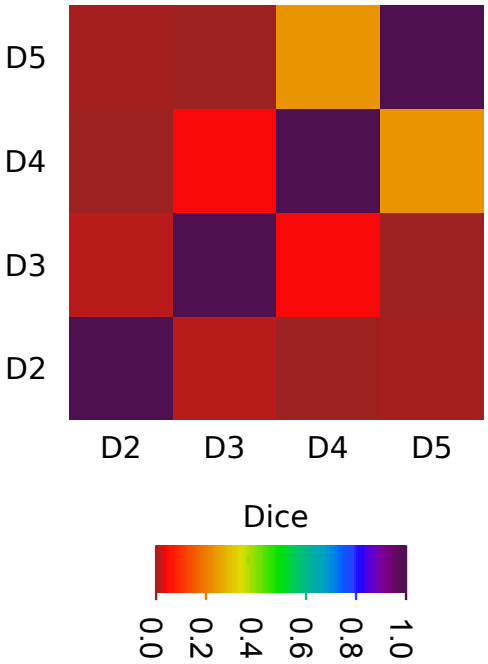

B Inter- versus intra-subject digit overlap patterns

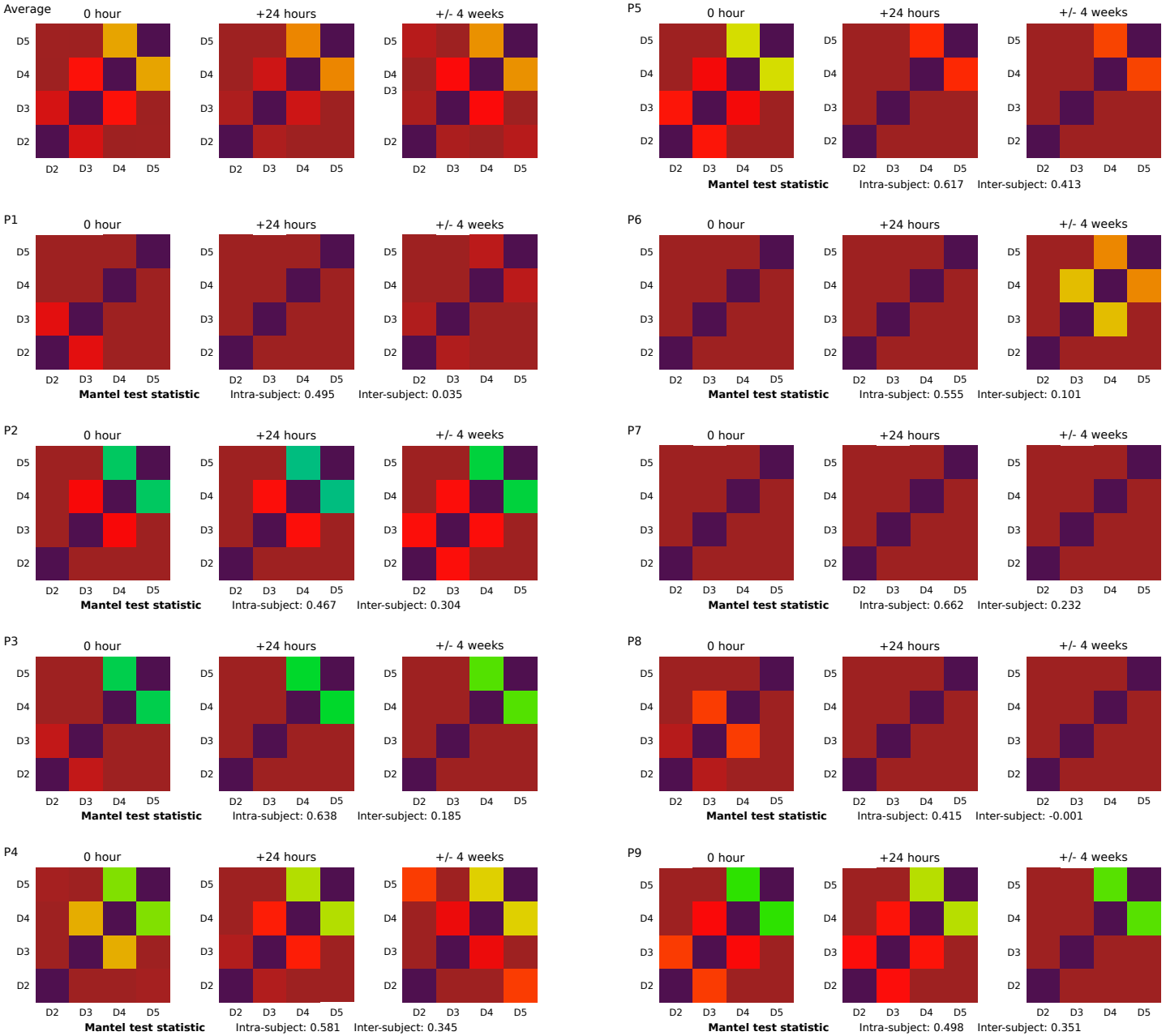

C Intra- versus inter-subject digit overlap similarity

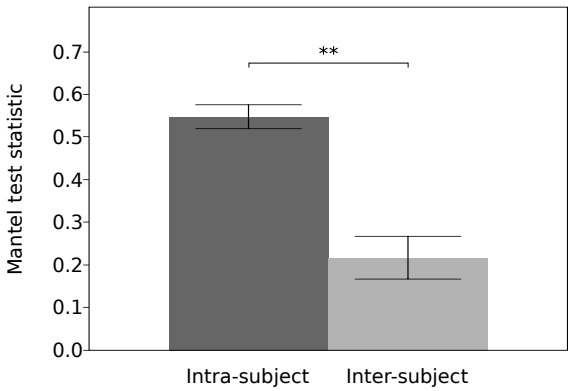

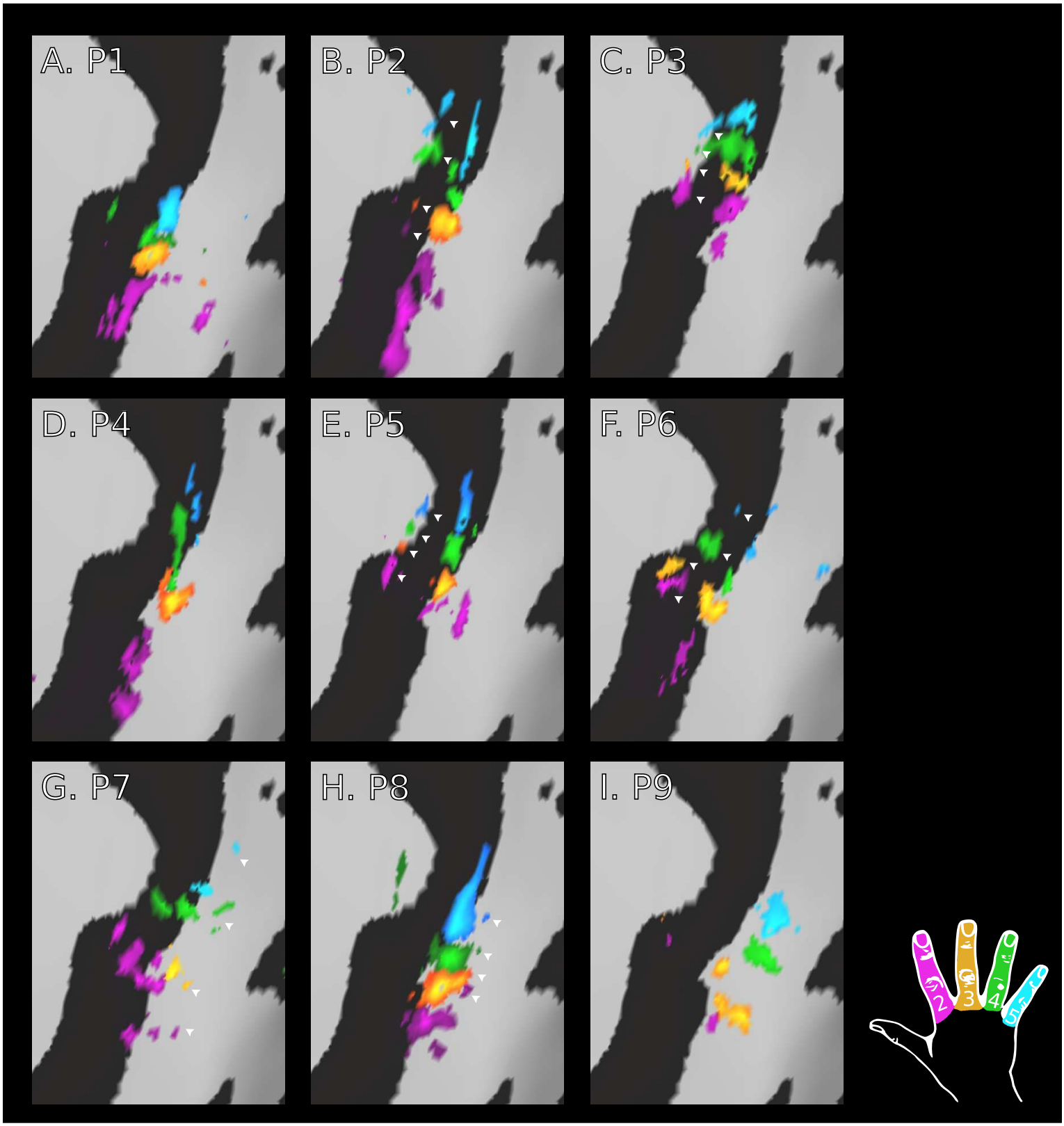
A. P1
B. P2
C. P3
D. P4
E. P5
F. P6
G. P7
H. P8
I. P9
1
2
3
4
5

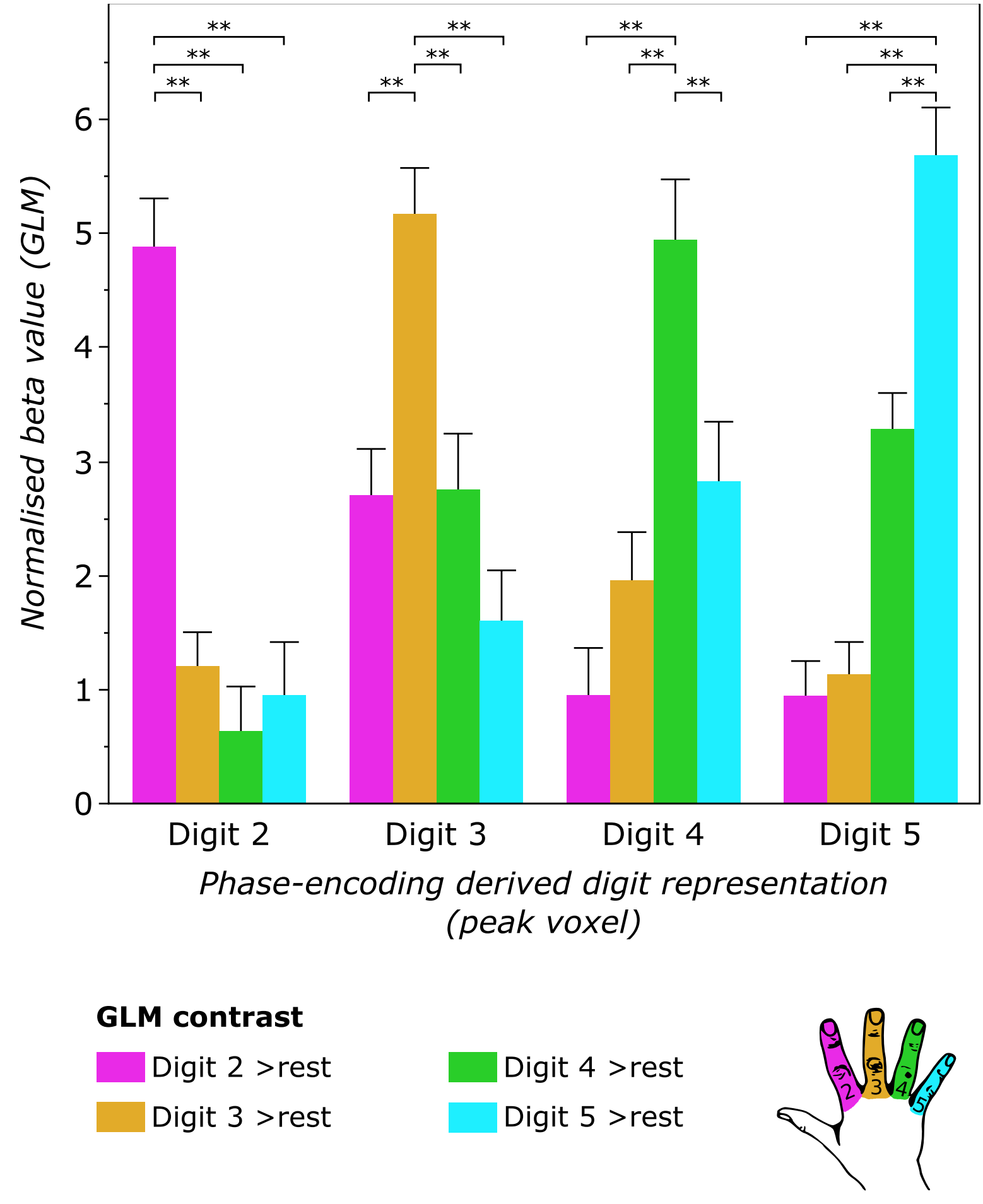
**
**
**
**
**
**
**
**
**
**
**
**
6
5
4
3
2
1
0
Normalised beta value (GLM)
Digit 2
Digit 3
Digit 4
Digit 5
Phase-encoding derived digit representation
(peak voxel)
GLM contrast
Digit 2 >rest
Digit 3 >rest
Digit 4 >rest
Digit 5 >rest
2
3
4